

# Influence of a Rising Bubble on the Behavior of the Slag-Steel Interface



Yong Liu, Shusen Cheng, and Wenxuan Xu

**Abstract** The interfacial contact area between molten steel and slag is one of the key factors influencing the efficiency of chemical reactions. This study reconstructs the phenomenon of gas bubbles traversing the slag-steel interface by constructing a physical model of the water–oil system and employing image processing techniques. The study focuses on the effects of bubble size, slag density, viscosity, and interfacial tension on the entrainment volume of steel and the slag-steel interface area. The entrainment volume increases with the increase of bubble size or slag density, but decreases with the increase of slag viscosity. The interface area shows a trend of first increasing and then decreasing with the increase of bubble size, and increases with the increase of slag density or the decrease of slag viscosity. As the oil-air interfacial tension increases, the water–air interfacial tension decreases, or the water–oil interfacial tension decreases, the liquid–liquid interface area increases.

**Keywords** Physical model · Mathematical simulation · Steel-slag interface · Rising bubble · Carried volume · Interfacial area

## Introduction

In metallurgical reaction processes, molten metal is often covered by a certain thickness of slag and accompanied by a gas stirring and mixing process. Consequently, the rising of bubbles from the metal to the slag is an inevitable process [1–3]. The passage of bubbles through the slag-steel interface effectively increases the interface area [3]. Also, this phenomenon can affect the efficiency of the slag-steel interface reaction [4–6].

---

Y. Liu (✉) · S. Cheng

School of Metallurgical and Ecological Engineering, University of Science and Technology, Beijing, Beijing 100083, China  
e-mail: [liuyong\\_ustb@126.com](mailto:liuyong_ustb@126.com)

W. Xu

Research Institute of Technology, Shougang Group Co., Ltd., Beijing 100043, China

© The Minerals, Metals & Materials Society 2024

S. Wagstaff et al. (eds.), *Materials Processing Fundamentals 2024*, The Minerals, Metals & Materials Series, [https://doi.org/10.1007/978-3-031-50184-5\\_7](https://doi.org/10.1007/978-3-031-50184-5_7)

In the 1960s, researchers [7] notice the phenomenon of bubbles at the slag-steel interface and conducted exploratory work. Han et al. [8–10] used X-ray transmission techniques to study the phenomenon of single bubbles passing through the slag-iron interface. The findings revealed that the entrainment of iron droplets increased with larger bubble sizes and decreased with rising interfacial tension and higher slag viscosity. Besides, researchers have indirectly studied the phenomenon of bubbles at the interface of immiscible liquid phases using physical simulation based on the principle of similarity. The factors such as bubble diameter [11–13], interfacial tension [11], fluid viscosity, and density [14–17] are considered to analyze their effects on the interface phenomenon. Díaz et al. [13] discovered that with the increase in bubble size, the volume of entrained heavier liquid phase also increases [12]. Tanno et al. [17] demonstrated that the amount of entrained heavier liquid phase decreases with the increase in density of the heavier liquid phase. The research conducted at the liquid-bubble interface, a liquid film carrying the heavier liquid phase is formed, and the flow rate of the liquid film around the bubble depends on viscosity, interfacial tension, and buoyancy effects between the liquids [18, 19].

In summary, the majority of research efforts have concentrated on analyzing the liquid column of the heavier liquid phase carried by bubbles and the volume of entrained liquid. Nevertheless, there is a scarcity of research addressing the alterations in interface area resulting from the process of bubble traversal. The purpose of this study is to investigate the motion behavior of bubbles at the liquid–liquid interface, reproduce the phenomenon of bubbles crossing the liquid–liquid interface, and specifically analyze the changes in interface area when bubbles of different sizes cross different upper liquid phases.

## Physics and Mathematical Models

### *Clod Model*

The physical experiments were conducted in a rectangular organic glass container with inner dimensions of 220 mm × 80 mm × 500 mm, as shown in Fig. 1. A planar light source is placed on one side of the organic glass container. The experimental recordings were captured using a high-speed color camera with a frame rate of 200 frames per second. The size of the bubbles during the experiment was controlled by a rotating axis connected to a circular holder. A specified volume of bubble was injected into the circular holder using a syringe, and then released by the rotating axis bearing.

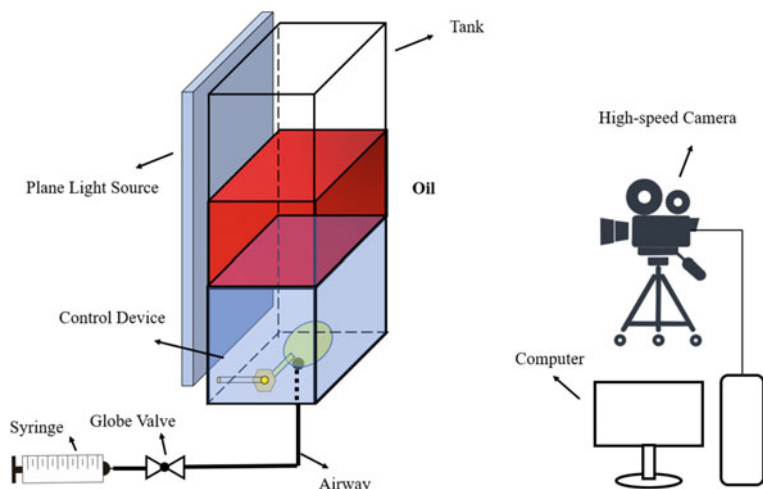


**Fig. 1** Experimental setup

**Table 1** Physical experimental fluid properties parameters

Parameter	Water	3# oil	Paraffin oil	100# oil	200# oil
Density/(g cm <sup>-3</sup> )	0.98	0.76	0.84	0.80	0.81
Viscosity/(mPa s)	3	8.9	9.6	93.3	193.5
Surface tension/(N m <sup>-1</sup> )	0.07	0.033	0.030	0.035	0.034
Water–oil interfacial tension/(N m <sup>-1</sup> )	–	0.040	0.040	0.042	0.047

## *Experimental Method*

During the experiment, the water level was kept constant, and the main focus was on the influence of the initial bubble diameter on the entrainment volume and the steel-sludge interface area when different types of oil simulated the slag layer. The key physical parameters are given in Table 1. In the experiment, each test group was repeated 5 times to reduce the accidental error in the experimental data.

## *Numerical Simulation*

In physical simulation experiments, although the phenomenon of bubbles passing through the slag metal interface can be reproduced, due to the properties of the experimental material, the effects of single factors such as fluid density, viscosity, and interfacial tension on the entrainment volume and slag metal interface area cannot be accurately determined. Therefore, numerical simulation methods are used

to analyze the impact of individual parameters. The assumptions and detailed control equations underlying the numerical simulation can be found in references [20, 21], which have been validated through physical models of water oil systems.

### Interface Area Analysis Method

As bubbles enter the slag phase from the metal solution, the steel-slag interface bulges upwards, forming peaks that can be tall, short, wide, or thin. To analyze this phenomenon, a rectangular coordinate system, as illustrated in Fig. 2a, was established. Coordinates at the liquid–liquid interface boundary were then extracted using GetData software, as depicted in Fig. 2b. This process enabled the derivation of the data relationship governing the liquid–liquid interface boundary, which was subsequently fitted to reconstruct the entrainment phenomenon.

In this study, the growth rate of the interface area is a crucial parameter used to assess changes in the interface area. The calculation of the interface area growth rate is denoted as  $\lambda$  and is determined using Eq. (1).

$$\lambda = (S_h - S_f)/S_f \tag{1}$$

where  $S_h$  and  $S_f$  represent the surface area of the bulging and initial liquid–liquid interface, respectively.

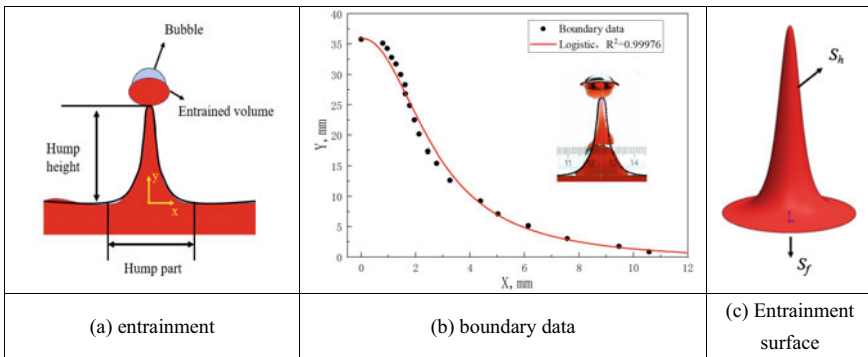


Fig. 2 Schematic diagram for extracting the interfacial area of a liquid–liquid interface

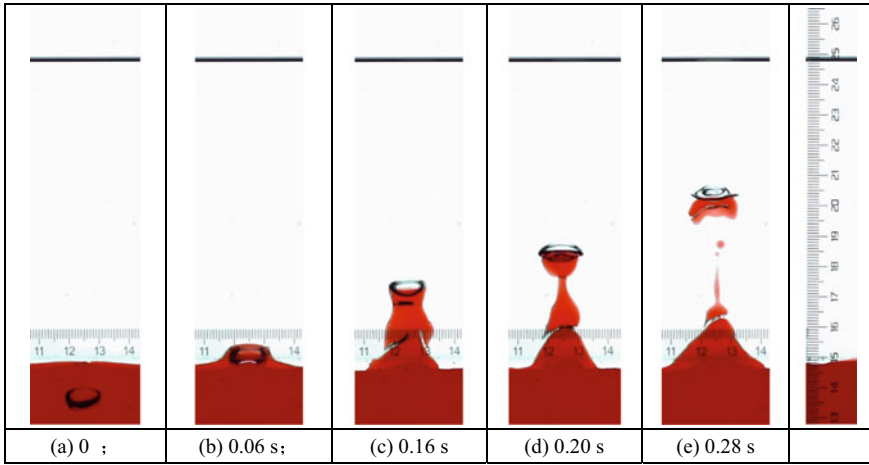


Fig. 3 Phenomenon of bubble ascent and entrainment process

## Results

### *The Entrainment Phenomenon*

The process of a bubble rising in a water-paraffin oil solution is depicted in Fig. 3. To emphasize the liquid–liquid interface, a water-soluble red dye was introduced into the water, enhancing the contrast between the two phases and making the evolving shapes between them during the ascent of the bubble more discernible. As evident in Fig. 3, the bubble is released in a static state. During its ascent, the bubble experiences deformation due to varying pressures in its vicinity. It continues to rise at a specific velocity until it reaches the interface between the liquid phases. Upon crossing this interface, a column of water forms beneath the bubble due to the wake effect. After reaching a certain height, this entrained water column detaches from the interface, breaking into two portions. One portion continues to ascend with the bubble, while the other descends back to the lower region.

### *Analysis of the Influence of the Entrainment Volume*

Figure 4 illustrates the relationship between entrainment volume and bubble size in various oil–water systems. The entrainment volume increases as the bubble diameter increases, but this relationship is nonlinear. In the 10# white oil–water system, with a 5 mm bubble size, the entrainment volume is 180 mm<sup>3</sup>. When the bubble size increases to 10, 15, 20, and 25 mm, the entrainment volume increases by 255.56%, 733.33%, 1866.67%, and 3611.11%, respectively, compared to the 5 mm bubble. Moreover,

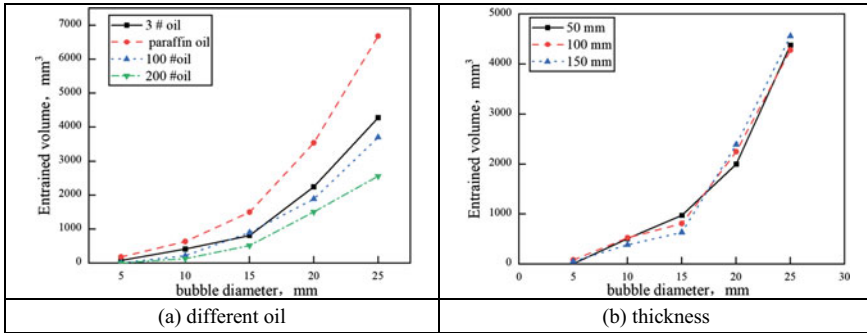


**Fig. 4** Relationship between bubbles of different sizes and entrained volume

the entrainment volume decreases as viscosity increases. For instance, with a 10 mm bubble size, the entrainment volume decreases by 65.63% and 78.91% as the oil phase viscosity increases from 9.6 to 93.3 mPa s and 193.5 mPa s, respectively. Furthermore, Fig. 4a indicates that within the range of studied oil layer thicknesses, there is no significant impact on the entrainment volume with varying oil layer thicknesses.

### *Analysis of the Influence of Slag-Steel Interface Area*

Physical simulation experiments were conducted to investigate the changes in the water–oil interface area induced by bubbles of different sizes, as depicted in Fig. 5. It is apparent from Fig. 5 that the alteration in the liquid–liquid interface area follows a pattern of initial increase followed by a subsequent decrease as the bubble diameter increases. Taking the paraffin oil–water system as an example, when the bubble size escalates from 5 mm to 10, 15, 20, and 25 mm, the growth rates of the liquid–liquid interface area increase by 81.80%, 312.98%, 130.00%, and 113.44%, respectively.

Figure 5a illustrates the influence of oil phase density and bubble diameter on the growth exponent of the interface area. As the oil phase density increases, the growth exponent of the interface area begins to decline. This reduction is attributed to the increased buoyancy as the water phase begins to penetrate the oil phase. Figure 5b presents the impact of oil phase viscosity on the interface area. As the oil phase viscosity decreases, the growth exponent of the interface area increases. For instance, when the initial bubble diameter is 15 mm, the growth rates of the interface area decrease by 10.99% and 31.39% as the oil phase viscosity increases from 9.6 to 93.3 mPa s and 193.5 mPa s, respectively.

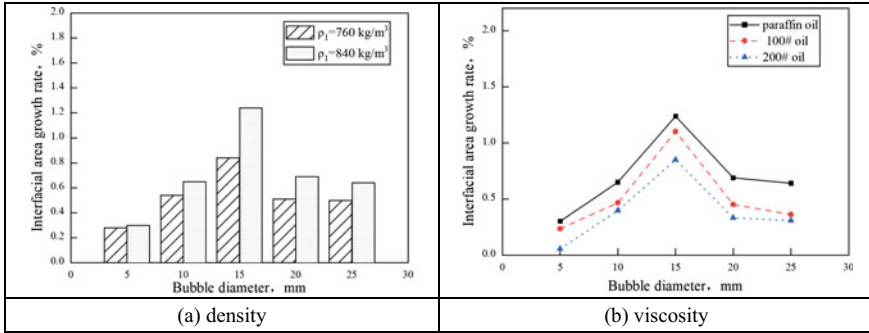


Fig. 5 Impact of light phase density and viscosity on interfacial area

### *Influence of the Interfacial Tension on the Interfacial Area of Slag-Steel*

In the numerical simulation scheme, the initial size of the bubble is 10 mm, and the parameters for the water phase and paraffin oil are described in Table 1. The numerical simulation results are shown in Fig. 6. The schematic diagram of the three-phase interface (water–oil–gas) during the bubble crossing process is shown in Fig. 6a–e. The three-dimensional display of the bubble rising process is shown in Fig. 6f. A comparison between physical and numerical simulations shows that the results are similar.

The variation in the liquid–liquid interface area during the bubble crossing process is depicted in Fig. 7, with a focus on the influence of interfacial tension. Observing Fig. 7a–c, it is evident that as the surface tension of the oil phase increases, leading to a reduction in the surface tension of water and consequently a decrease in the interfacial

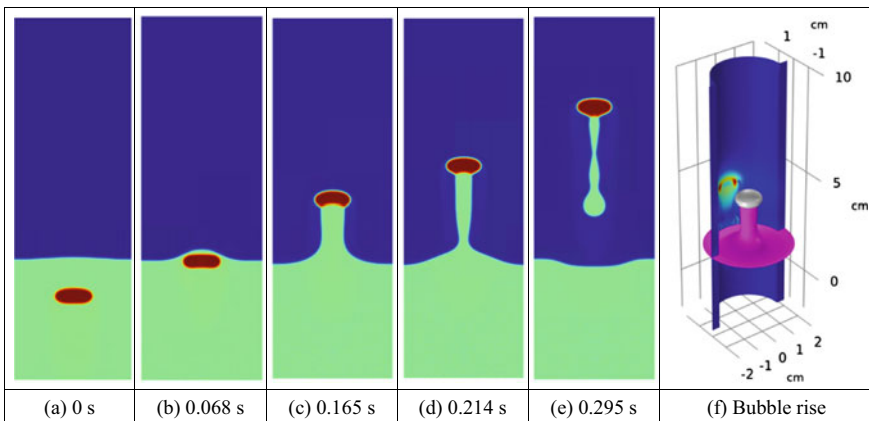
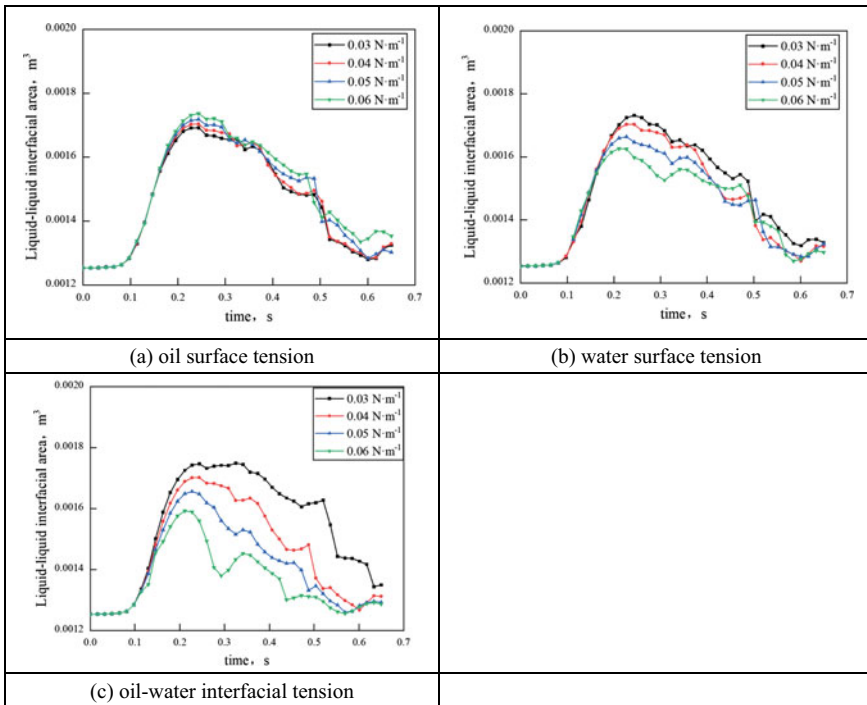


Fig. 6 Mathematical results

tension between water and oil, the interface area expands. Specifically, when the surface tension of the oil phase increases from 0.03 N/m to 0.04, 0.05, and 0.06 N/m, the maximum interface area increases by 0.59%, 1.78%, and 2.96%, respectively, compared to the base value of 0.03 N/m. Conversely, when the surface tension of water increases from 0.03 N/m to 0.04, 0.05, and 0. N/m, the maximum interface area decreases by 1.62%, 3.86%, and 6.05%, respectively. Figure 7c highlights the impact of oil–water interfacial tension on the interface area. As the oil–water interfacial tension increases, the resistance to bubble motion during the crossing of the liquid–liquid interface intensifies, leading to a reduction in the interface area. Specifically, when the oil–water interfacial tension increases by 33.33%, 66.67%, and 100.00% relative to the base value of 0.03 N/m, the maximum interface area decreases by 2.86%, 5.14%, and 9.14%, respectively.

The analysis above reveals that the interfacial tensions between water–oil–gas phases affect the water–oil interface area during the process of bubble crossing, with the degree of influence ranked as follows: water–oil interfacial tension, water–air interfacial tension, and oil–air interfacial tension.



**Fig. 7** Effect of interfacial tension on the interfacial area



## Conclusions

- (1) There is a nonlinear relationship between bubble size growth and entrainment, and as the bubble size increases, the rate of entrainment also increases sharply. Furthermore, the entrainment volume increases with the increase of oil density or the decrease of oil viscosity. However, within the studied range of oil layer thickness, the impact on entrainment is relatively small.
- (2) The interface area between the liquid–liquid phases shows a trend of increasing first and then decreasing as the bubble size increases. Meanwhile, when the density of the oil phase decreases or the viscosity increases, it has an inhibitory effect on the upward bulging of the liquid–liquid interface, restricting the growth rate of the interface area.
- (3) The interface area between the liquid–liquid phases increases as the surface tension of the oil phase increases, the surface tension of the water phase decreases, or the interfacial tension between water and oil decreases. The degree of influence on the interface area is ranked as follows: water–oil interfacial tension, water–air interfacial tension, and oil–air interfacial tension.

## References

1. Fabritius T, Riipi J, Järvinen M, Mattila O, Heikkinen E-P, Kärnä A, Kurikkala J, Sulasalmi P, Härkki J (2010) Interfacial phenomena in metal–slag–gas system during AOD process. *ISIJ Int* 50(6):797–803
2. Beskow K, Dayal P, Björkvall J, Nzotta M, Sichen D (2006) A new approach for the study of slag–metal interface in steelmaking. *Ironmaking Steelmaking* 33(1):74–80
3. Ekengård J, Andersson AMT, Jönsson PG (2008) Distribution of metal droplets in top slags during ladle treatment. *Ironmaking Steelmaking* 35(8):575–588
4. Yoshida H, Liu J, Kim S-J, Gao X, Ueda S, Kitamura S (2016) Influence of the interfacial tension on the droplet formation by bubble rupture in Sn(Te) and salt system. *ISIJ Int* 56(11):1902–1909
5. Kitamura S, Zeze M, Nakashima J (2016) Multi-phase flow of liquid/liquid system in steelmaking process. *Jpn J Multiphase Flow* 30(3):266–273
6. Song D-Y, Maruoka N, Maeyama T, Shibata H, Kitamura S (2010) Influence of bottom bubbling condition on metal emulsion formation in lead-salt system. *ISIJ Int* 50(11):1539–1545
7. Poggi D, Minto R, Davenport WG (1969) Mechanisms of metal entrapment in slags. *JOM* 21(11):40–45
8. Han Z, Holappa L (2003) Mechanisms of iron entrainment into slag due to rising gas bubbles. *ISIJ Int* 43(3):292–297
9. Han Z, Holappa L (2003) Bubble bursting phenomenon in gas/metal/slag systems. *Metall and Mater Trans B* 34(5):525–532
10. Han Z, Holappa L (2003) Characteristics of iron entrainment into slag due to rising gas bubbles. *ISIJ Int* 43(11):1698–1704
11. Greene GA, Chen JC, Conlin MT (1988) Onset of entrainment between immiscible liquid layers due to rising gas bubbles. *Int J Heat Mass Transf* 31(6):1309–1317
12. Mercier JL, da Cunha FM, Teixeira JC, Scofield MP (1974) Influence of enveloping water layer on the rise of air bubbles in Newtonian fluids. *J Appl Mech* 41(1):29–34
13. Díaz-Damacillo L, Ruiz-Angulo A, Zenit R (2016) Drift by air bubbles crossing an interface of a stratified medium at moderate Reynolds number. *Int J Multiphase Flow* 85:258–266

14. Choi K, Park H (2021) Interfacial phenomena of the interaction between a liquid–liquid interface and rising bubble. *Exp Fluids* 62(6):1–21
15. Pierson J-L, Magnaudet J (2018) Inertial settling of a sphere through an interface. Part 1. From sphere flotation to wake fragmentation. *J Fluid Mech* 835:762–807
16. Zhao H, Wang J, Zhang W, Xie M, Liu F, Cao X (2019) Bubble motion and interfacial phenomena during bubbles crossing liquid–liquid interfaces. *Processes* 7(10), Article 10
17. Tanno M, Liu J, Gao X, Kim S-J, Ueda S, Kitamura S (2017) Influence of the physical properties of liquids and diameter of bubble on the formation of liquid column at the interface of two liquid phases by the rising bubble. *Metall and Mater Trans B* 48(6):2913–2921
18. Mao N, Kang C, Teng S, Mulbah C (2020) Formation and detachment of the enclosing water film as a bubble passes through the water-oil interface. *Colloids Surf, A* 586:124236
19. Rozario A, Viswanathan NN, Basu S (2019) Rise of gas bubbles across the interface between two liquids. *Metall and Mater Trans B* 50(1):10–15
20. Zhou XB, Zhao ZS, Wang WX, Xu JG, Yue Q (2023) Physical and mathematical simulation on the bubble entrainment behavior at slag-metal interface. *Acta Metallurgica Sinica Online First*, 1–12
21. Farhadi J, Sattari A, Hanafizadeh P (2022) Passage of a rising bubble through a liquid-liquid interface: a flow map for different regimes. *Can J Chem Eng* 100(2):375–390